

Photoacoustic monitoring of blood oxygenation during neurosurgical interventions

Thomas Kirchner^{1,2,*}, Janek Gröhl^{1,3}, Niklas Holzwarth^{1,2}, Mildred A. Herrera⁴, Tim Adler^{1,5}, Adrián Hernández-Aguilera⁴, Edgar Santos⁴, Lena Maier-Hein^{1,3}

- 1** Division of Computer Assisted Medical Interventions, German Cancer Research Center, Heidelberg, Germany.
2 Faculty of Physics and Astronomy, Heidelberg University, Heidelberg, Germany.
3 Medical Faculty, Heidelberg University, Heidelberg, Germany.
4 Department of Neurosurgery, Heidelberg University Hospital, Heidelberg, Germany.
5 Faculty of Mathematics and Computer Science, Heidelberg University, Heidelberg, Germany.

* Please address your correspondence to Thomas Kirchner, e-mail: t.kirchner@dkfz-heidelberg.de

Abstract

Multispectral photoacoustic (PA) imaging is a prime modality to monitor hemodynamics and changes in blood oxygenation (sO_2). Although sO_2 changes can be an indicator of brain activity both in normal and in pathological conditions, PA imaging of the brain has mainly focused on small animal models with lissencephalic brains. Therefore, the purpose of this work was to investigate the usefulness of multispectral PA imaging in assessing sO_2 in a gyrencephalic brain. To this end, we continuously imaged a porcine brain as part of an open neurosurgical intervention with a handheld PA and ultrasonic (US) imaging system *in vivo*. Throughout the experiment, we varied respiratory oxygen and continuously measured arterial blood gases. The arterial blood oxygenation (SaO_2) values derived by the blood gas analyzer were used as a reference to compare the performance of linear spectral unmixing algorithms in this scenario. According to our experiment, PA imaging can be used to monitor sO_2 in the porcine cerebral cortex. While linear spectral unmixing algorithms are well-suited for detecting changes in oxygenation, there are limits with respect to the accurate quantification of sO_2 , especially in depth. Overall, we conclude that multispectral PA imaging can potentially be a valuable tool for change detection of sO_2 in the cerebral cortex of a gyrencephalic brain. The spectral unmixing algorithms investigated in this work will be made publicly available as part of the open-source software platform Medical Imaging Interaction Toolkit (MITK).

1 Introduction

A major application of photoacoustic (PA) imaging is the monitoring of hemodynamics and changes in blood oxygenation (sO_2) [1], which are indicators of brain activity [2, 3] or injury [4]. In clinical practice, techniques for the monitoring of brain injury can vary widely with the specific application. While there are various techniques that can image hemodynamics, PA imaging can potentially provide better functional information and higher resolution [5]. sO_2 is usually calculated via the estimation of abundances of oxygenated and deoxygenated hemoglobin chromophores [6]. In multispectral PA imaging, this concentration estimation is generally done by linear spectral unmixing (SU) [7, 8, 9], which involves solving a set of linear equations for the desired abundances of hemoglobin [10]. While PA imaging is widely used in small animal models with lissencephalic brains, larger and more complex brains remain challenging [5]. The purpose of this work was therefore to investigate the usefulness of multispectral PA imaging in assessing sO_2 in a gyrencephalic brain.

2 Material and Methods

To investigate the performance of sO_2 estimation by SU *in vivo* in a neurosurgical setting, we performed PA measurements during an open intervention on a porcine brain, which allowed us to image without the acoustic attenuation of the skull. In this setting, we were also able to take corresponding arterial blood gas (ABG) [11] measurements and thus to compare the quantitative sO_2 estimation performance of numerical algorithms for SU [12], against a physiological arterial blood oxygenation (SaO_2) reference value.

Experimental setup

The PA imaging modality used in this study was a custom hybrid PA and ultrasonic (US) system with a fast-tunable optical parametric oscillator (OPO) laser system (Phocus Mobile, Oportek, Carlsbad, USA) and a 7.5 MHz linear US transducer with 128 elements (L7-Xtech, Vermon, Tours, France), on a DiPhAs ultrasonic research platform (Fraunhofer IBMT, St. Ingbert, Germany) [13]. The custom probe holder covered the transducer with a gold leaf to reduce transducer absorption artifacts. For optimal contrast to noise [14], the PA images were recorded at 760 nm and 858 nm, adding 798 nm as an isosbestic reference.

A porcine brain was continuously imaged for 45 min, as part of an open neurosurgical intervention with our hybrid PA and US probe. Our experiment was carried out following a craniotomy on a three month old female domestic pig. As illustrated in Figure 1a, the probe was fixed over the left hemisphere of the brain to record a sagittal slice, using a gel pad as acoustic coupling. During imaging, the ventilation of the animal was varied and SaO_2 and reference measurements with an ABG analyzer were taken. The ventilation changes and reference measurements are detailed in Figure 2 and Table 1. In addition, SaO_2 was monitored non-invasively with a pulse oximeter [15] placed on the left earlobe.

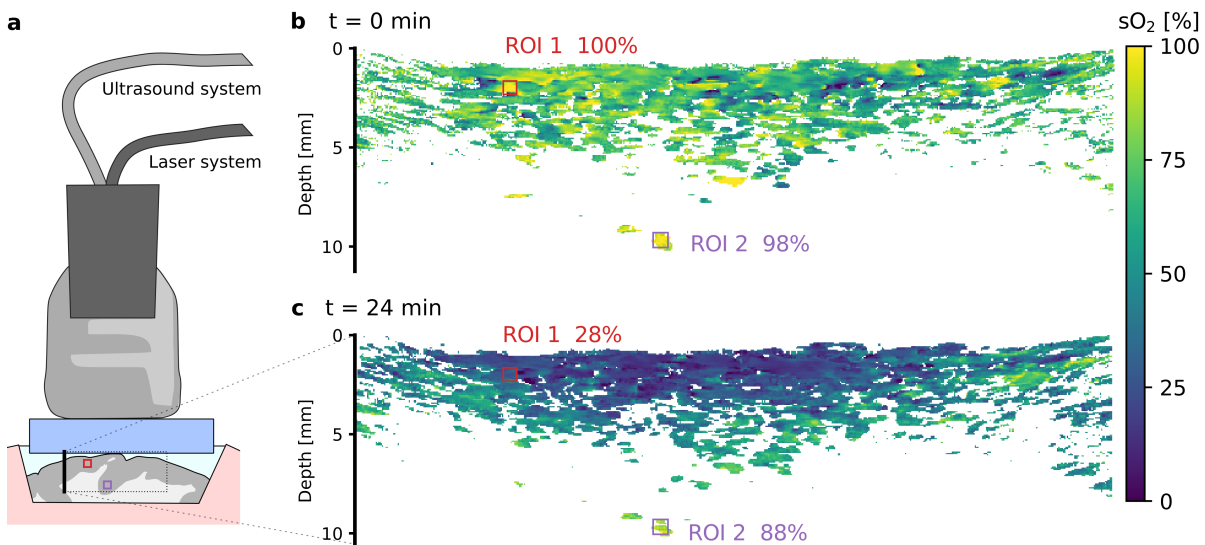


Figure 1: (a) Experimental setup. The photoacoustic (PA) probe was used to record sagittal images of a porcine brain. The field of view contains two regions of interest (ROIs) corresponding to arteries near (ROI1 – red) and far (ROI2 – purple) from the brain surface. (b) & (c) Example images of blood oxygenation (sO_2) in a brain slice. The ROIs are annotated with their corresponding median sO_2 value as determined with the Householder QR unmixing algorithm. t is the time from start of the experiment. In both sO_2 images, values under a noise equivalent threshold of unmixed total hemoglobin were masked. In (b) the respiratory oxygen (rO_2) was 35% and arterial blood gas (ABG) analysis yielded an arterial blood oxygenation (SaO_2) of 100%, while in (c) rO_2 was 0% with $\text{SaO}_2 = 26.2\%$.

Image processing

Using the Medical Interaction Toolkit (MITK) [16] PA image processing plugin [17], the raw PA data was beamformed with delay and sum [18, 19] and von Hann apodization. The resulting images were motion corrected with the corresponding US B-mode images. All input images were averaged over ten recordings per wavelength before linear SU, which was performed on the PA images with five commonly used linear algorithms [20]. To cover a wide range of algorithms, we selected a QR decomposition with Householder transformation [21], a LU (with full pivoting) [22] and a singular value decomposition [23] all from the C++ *Eigen* [24] library, as well as a weighted [25] (based on QR decomposition) and a non-negative (using least angle regression [26]) least square algorithm both from the C++ *Vigra* [27] library.

For quantitative validation of the SU algorithms, we selected two regions of interest (ROIs), for which

we determined sO_2 values. We selected a surface ROI and a deep one to investigate the influence of fluence effects [28] on SU sO_2 estimation. We assumed that both ROIs contain arteries, as they had generally high PA signal and distinct characteristic pulsing in the US and PA image streams. The resulting sO_2 values for one ROI are the median of all pixels within that ROI that have a higher than noise equivalent total hemoglobin level.

3 Results and Discussion

According to our results in Table 1, the different SU algorithms were similar in estimation performance, with the exception of the non-negative least square boundary effect. While other algorithms can yield physiologically impossible sO_2 values (even above 100%, and theoretically also below 0%), the non-negativity constraint artificially prevents this. This was especially relevant for the evaluation of changes in ROI2. All other differences between the algorithms are within their respective standard deviations. The Householder QR algorithm performed the fastest. In the following, we therefore only present the SU results of the QR algorithm. Example slices are shown in Figure 1b&c with the marked ROIs and their corresponding median sO_2 value.

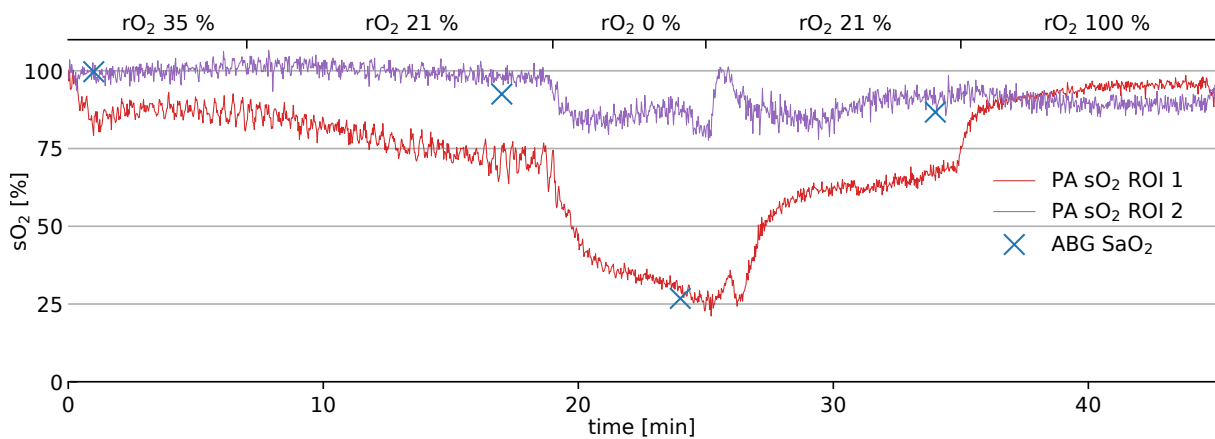


Figure 2: Photoacoustic blood oxygenation (sO_2) estimation over time in two regions of interest (ROIs) (see Figure 1). The different levels of respiratory oxygen (rO_2) delivered by the ventilation are displayed above the plot; the arterial blood gas (ABG) reference measurements of arterial blood oxygenation (SaO_2) as blue crosses.

Comparing the changes in ventilation with the time course characteristics of the unmixing results of ROI1 in Figure 2, one can see that linear SU can be used for change detection of sO_2 in the cerebral cortex. However, the unmixing results do not closely follow the quantitative values of the ABG reference (Table 1). This illustrates the limits in quantification of sO_2 with PA imaging and is even more obvious in deep tissue, considering the small changes in sO_2 estimation for ROI2.

In conclusion, our study suggests that PA imaging can be used to monitor sO_2 changes in the cerebral cortex during neurosurgical interventions. However, care must be taken when interpreting sO_2 estimation results due to the limits in quantitative accuracy when using linear SU algorithms. This is especially relevant in deep tissue due to fluence dependent spectral coloring. While there are promising approaches to address these fluence effects in general [29, 30, 31] and spectral coloring specifically [28], the translation of quantitative PA imaging deep in tissue remains a major challenge.

Acknowledgements

The authors would like to acknowledge support from the European Union through the ERC starting grant COMBIOSCOPY under the New Horizon Framework Programme grant agreement ERC-2015-StG-37960. The animal experiment was approved by the institutional animal care and use committee in Karlsruhe, Baden-Württemberg, Germany; under Protocol No. 35-9185.81/G-174/16.

time [min]	rO ₂ [%]	SaO ₂ [%]		QR/SVD sO ₂ [%]		LU sO ₂ [%]		NNLS sO ₂ [%]		WLS sO ₂ [%]	
		ABG	PuOx	ROI 1	ROI 2	ROI 1	ROI 2	ROI 1	ROI 2	ROI 1	ROI 2
+0	35	100	99	85 ± 2	99 ± 2	85 ± 2	98 ± 2	85 ± 2	98 ± 2	85 ± 2	98 ± 2
+8	21	93	88-92	72 ± 3	98 ± 2	72 ± 4	98 ± 2	72 ± 3	98 ± 1	72 ± 3	98 ± 2
+24	0	26	40	27 ± 2	84 ± 3	26 ± 2	83 ± 4	27 ± 2	84 ± 3	27 ± 2	84 ± 3
+34	21	86	–	69 ± 2	91 ± 3	69 ± 2	91 ± 3	69 ± 2	91 ± 3	69 ± 2	91 ± 3
+45	100	–	100	95 ± 2	91 ± 2	95 ± 2	90 ± 2	95 ± 2	91 ± 2	95 ± 2	90 ± 2

Table 1: Comparison of the arterial blood gas (ABG), pulse oximetry (PuOx) and five spectral unmixing (SU) estimations – in region of interest (ROI) 1 & 2. Values are averaged over one minute beginning at the time after start of the recording. The respiratory oxygen (rO₂) value was adjusted at least five minutes before the recording (see Figure 2). SVD: singular value decomposition, NNLS: non-negative least squares, WLS: weighted least squares. –: Missing values failed to record due to technical issues.

References

- [1] Wang, L. V. & Hu, S. Photoacoustic tomography: in vivo imaging from organelles to organs. *Science* **335**, 1458–1462 (2012).
- [2] Fransson, P. Spontaneous low-frequency bold signal fluctuations: An fMRI investigation of the resting-state default mode of brain function hypothesis. *Human brain mapping* **26**, 15–29 (2005).
- [3] Raichle, M. E. *et al.* A default mode of brain function. *Proceedings of the National Academy of Sciences* **98**, 676–682 (2001).
- [4] Takano, T. *et al.* Cortical spreading depression causes and coincides with tissue hypoxia. *Nature Neuroscience* **10**, 754 (2007).
- [5] Yao, J. & Wang, L. V. Photoacoustic brain imaging: from microscopic to macroscopic scales. *Neurophotonics* **1**, 011003 (2014).
- [6] Jobsis, F. F. Noninvasive, infrared monitoring of cerebral and myocardial oxygen sufficiency and circulatory parameters. *Science* **198**, 1264–1267 (1977).
- [7] Keshava, N. & Mustard, J. F. Spectral unmixing. *IEEE signal processing magazine* **19**, 44–57 (2002).
- [8] Li, M.-L. *et al.* Simultaneous molecular and hypoxia imaging of brain tumors in vivo using spectroscopic photoacoustic tomography. *Proceedings of the IEEE* **96**, 481–489 (2008).
- [9] Gerling, M. *et al.* Real-time assessment of tissue hypoxia in vivo with combined photoacoustics and high-frequency ultrasound. *Theranostics* **4**, 604 (2014).
- [10] Chance, B. *et al.* Comparison of time-resolved and-unresolved measurements of deoxyhemoglobin in brain. *Proceedings of the National Academy of Sciences* **85**, 4971–4975 (1988).
- [11] McFadden Jr, E. & Lyons, H. A. Arterial-blood gas tension in asthma. *New England Journal of Medicine* **278**, 1027–1032 (1968).
- [12] Tzoumas, S., Deliolanis, N., Morscher, S. & Ntziachristos, V. Unmixing molecular agents from absorbing tissue in multispectral optoacoustic tomography. *IEEE transactions on medical imaging* **33**, 48–60 (2014).
- [13] Kirchner, T., Wild, E., Maier-Hein, K. H. & Maier-Hein, L. Freehand photoacoustic tomography for 3d angiography using local gradient information. In *Photons Plus Ultrasound: Imaging and Sensing 2016*, vol. 9708, 97083G (International Society for Optics and Photonics, 2016).
- [14] Luke, G. P., Nam, S. Y. & Emelianov, S. Y. Optical wavelength selection for improved spectroscopic photoacoustic imaging. *Photoacoustics* **1**, 36–42 (2013).
- [15] Tremper, K. K. Pulse oximetry. *Chest* **95**, 713–715 (1989).

-
- [16] Nolden, M. *et al.* The medical imaging interaction toolkit: challenges and advances. *International journal of computer assisted radiology and surgery* **8**, 607–620 (2013).
- [17] Kirchner, T., Sattler, F., Gröhl, J. & Maier-Hein, L. Signed real-time delay multiply and sum beamforming for multispectral photoacoustic imaging. *Journal of Imaging* **4**, 121 (2018).
- [18] Griffiths, L. & Jim, C. An alternative approach to linearly constrained adaptive beamforming. *IEEE Transactions on antennas and propagation* **30**, 27–34 (1982).
- [19] Kim, J. *et al.* Programmable real-time clinical photoacoustic and ultrasound imaging system. *Scientific reports* **6**, 35137 (2016).
- [20] Burden, R. L., Faires, J. D. & Reynolds, A. C. Numerical analysis (2001).
- [21] Goodall, C. R. *13 Computation using the QR decomposition* (Elsevier, 1993).
- [22] Adomian, G. A review of the decomposition method in applied mathematics. *Journal of mathematical analysis and applications* **135**, 501–544 (1988).
- [23] Boardman, J. W. Inversion of imaging spectrometry data using singular value decomposition. In *12th Canadian Symposium on Remote Sensing Geoscience and Remote Sensing Symposium* (1989).
- [24] Guennebaud, G. *et al.* Eigen v3 (2010).
- [25] Shimabukuro, Y. E. & Smith, J. A. The least-squares mixing models to generate fraction images derived from remote sensing multispectral data. *IEEE Transactions on Geoscience and Remote sensing* **29**, 16–20 (1991).
- [26] Efron, B., Hastie, T., Johnstone, I., Tibshirani, R. *et al.* Least angle regression. *The Annals of statistics* **32**, 407–499 (2004).
- [27] Köthe, U. Vision with generic algorithms (vgra). <https://ukoethe.github.io/vgra/> (2018).
- [28] Tzoumas, S. *et al.* Eigenspectra optoacoustic tomography achieves quantitative blood oxygenation imaging deep in tissues. *Nature communications* **7**, ncomms12121 (2016).
- [29] Kirchner, T., Gröhl, J. & Maier-Hein, L. Context encoding enables machine learning-based quantitative photoacoustics. *Journal of biomedical optics* **23**, 056008 (2018).
- [30] Hänninen, N., Pulkkinen, A. & Tarvainen, T. Image reconstruction with reliability assessment in quantitative photoacoustic tomography. *Journal of Imaging* **4**, 148 (2018).
- [31] Gröhl, J., Kirchner, T., Adler, T. & Maier-Hein, L. Confidence estimation for machine learning-based quantitative photoacoustics. *Journal of Imaging* **4**, 147 (2018).